Available online at https://link.springer.com/journal/42241
http://www.jhydrodynamics.com
Journal of Hydrodynamics, 2026
https://doi.org/10.1007/s42241-026-0045-6

Numerical investigation of generic submarine self-propulsion in free-surface waves with an autopilot controller

Yu-heng Sun[1], Jie Zhu[2], Liu-shuai Cao[1*], De-cheng Wan[1]

1. *Computational Marine Hydrodynamics Lab (CMHL), School of Ocean and Civil Engineering, Shanghai Jiao Tong University, Shanghai 200240, China*
2. *Wuhan Second Ship Design and Research Institute, Wuhan 430064, China*

(Received January 13, 2026, Revised March 11, 2026, Accepted March 15, 2026, Published online June 16, 2026)

Abstract: This study employs computational fluid dynamics (CFD) to investigate the attitude-keeping self-propulsion of a generic submarine in free-surface and wave environments under autopilot control. The Joubert BB2 hull form and Marine 7371R propeller are adopted as the reference models. Turbulent flow is resolved by solving the incompressible Reynolds averaged Navier-Stokes (RANS) equations in combination with the shear stress transport (SST) k-ω turbulence model, while free-surface dynamics are captured using the volume of fluid (VOF) method. To ensure numerical reliability, mesh-convergence studies are carried out with four levels of mesh resolution. An overset mesh technique is applied to the submarine hull and X-rudders, whereas a sliding mesh is used to represent propeller rotation. The autopilot is implemented as a proportional-derivative (PD) controller that adjusts attitude variables to maintain attitude-keeping self-propulsion. The influence of submergence depth and wave conditions on hydrodynamic characteristics is systematically examined: The presence of the free surface significantly alters the hydrodynamic loads, surface pressure distribution, and associated wave patterns during the self-propulsion process. Meanwhile, the wave action induces significant variations in the pitch angle, leading to distinct periodic oscillations in the submarine's attitude.

Key words: Submarine, computational fluid dynamics (CFD), near-surface, self-propulsion, overset mesh

0. Introduction

Self-propulsion is a fundamental aspect of submarine operation, influencing both its performance and efficiency, particularly in near-surface environments. Under these conditions, the free surface significantly impacts the flow dynamics around the submarine, affecting both propulsion and maneuverability. Understanding these interactions is critical for optimizing submarine design and enhancing operational capabilities.

Submarine self-propulsion has been extensively studied through experimental investigations to understand the interaction between the hull and propeller in various operating conditions[1-2]. The DARPA SUBOFF, a widely used generic submarine model, has been the subject of numerous studies in both model testing and numerical simulations. Overpelt et al.[3] provided experimental data on the maneuvering performance of a modern SSK-class submarine, validating numerical methods for studying submarine maneuvering and self-propulsion in both model and full-scale configurations. Özden et al.[4] conducted a detailed experimental and numerical study on the DARPA SUBOFF, using the INSEAN E1619 propeller to explore self-propulsion characteristics and validate computational fluid dynamics (CFD) methods for predicting submarine performance. Similarly, Wang et al.[5] investigated the propeller wake of a generic submarine in near-surface conditions, noting how free-surface proximity alters the wake structure and impacts overall propulsion efficiency. These experimental studies laid the groundwork for understanding submarine self-propulsion, yet they highlighted the challenges in accurately capturing the free-surface effects in traditional model testing.

As a result, CFD has become increasingly essential in advancing the understanding of submarine dynamics. Recent advances in numerical methods

Project supported by the National Natural Science Foundation of China (Grant Nos. 52571360, 52131102).
Biography: Yu-heng Sun (2002-), Male, Master,
E-mail: sun_yuheng@sjtu.edu.cn
Corresponding author: Liu-shuai Cao,
E-mail: liushuaicao@sjtu.edu.cn

have made it possible to simulate submarine self-propulsion more accurately, particularly in near-surface environments. Bai et al.[6] investigated submarine self-propulsion using different turbulence models, examining the effects of these models on the accuracy of CFD simulations for predicting submarine performance under various hydrodynamic conditions. The introduction of two-equation eddy-viscosity turbulence models by Menter[7] has become a standard tool for simulating turbulent flows around submarines and their propellers. Liefvendahl and Troëng[8] further refined turbulence modeling by applying large eddy simulation (LES) to study cycle-to-cycle variations in blade loads for submarine propellers, improving the understanding of transient forces and unsteady behavior in submarine propulsion. Posa and Balaras[9] applied LES to simulate the interaction between the propeller wake and hull during self-propulsion, providing insights into the complex hydrodynamic interactions that occur during submarine motion. Carrica et al.[10] extended this work by further studying complex and surface maneuvers of generic submarines in calm water, comparing with experimental data to verify the accuracy of CFD in simulating complex maneuvers. Lungu[11] used detached eddy simulation (DES) to investigate the flow dynamics around the DARPA SUBOFF in deep immersion and near-surface conditions, focusing on the role of submergence depth in hydrodynamic performance.

The accurate representation of propeller effects in self-propulsion simulations is essential for obtaining reliable numerical predictions. Chase and Carrica[12] investigated the contribution of the propeller to the self-propulsion performance of the DARPA SUBOFF and highlighted the importance of using sufficiently accurate CFD models to capture the interaction between the propeller and the submarine hull. Sezen et al.[13] conducted a Reynolds Averaged Navier-Stokes (RANS)-based CFD investigation of the self-propulsion performance of the benchmark DARPA SUBOFF model equipped with the E1619 propeller. Their study incorporated verification and validation procedures for both the bare/appended hull resistance and open-water propeller performance, and further evaluated the propeller–hull interaction at the self-propulsion point, demonstrating the importance of numerical accuracy in reliably predicting the self-propulsive behavior of underwater vehicles.

In addition to propeller hydrodynamics, the dynamic response of submarine maneuvering has also become a central topic in CFD research. Cheng et al.[14] validated, by means of CFD, the large-amplitude motion response of the hull under internal-wave conditions. At the same time, as underwater missions grow increasingly complex and maneuverability requirements become more stringent, research on submarine autopilot controller has attracted widespread attention in the hydrodynamics community. It enables control over essential navigational parameters such as heading, depth, attitude, and speed. Kim[15] developed a six-degrees-of-freedom simulation framework incorporating an autopilot controller to investigate the motion response and maneuvering characteristics of an underwater vehicle, thereby providing valuable insight into the response mechanisms to control commands during complex maneuvers. Han et al.[16] extended this research by simulating turning maneuvers of underwater vehicles, analyzing the hydrodynamic forces involved in achieving stable turns. In recent years, increasing attention has been paid to the hydrodynamic performance of submarines operating in the vicinity of the free surface. Cao et al.[17] investigated the hydrodynamic performance and wake characteristics of a submarine navigating near the free surface in a continuously stratified fluid, with the primary objective of elucidating the influence of density stratification on hydrodynamic loads, free-surface disturbances, and wake evolution. In the context of near-surface maneuvers, Guo et al.[18] numerically investigated the turning motion of a near-surface self-propelled submarine using a RANS-volume of fluid (VOF) framework. Their study revealed that variations in submergence depth significantly affect the free- surface wave pattern, shedding vortices, and velocity distribution around the submarine, thereby modifying its near-surface maneuvering characteristics. Chen et al.[19] studied the numerical simulation of near-surface turn maneuvers of a generic submarine, highlighting the influence of free-surface waves on turning behavior. Guo et al.[20] conducted a similar investigation into the steady turning motion of a submarine near the free surface, showing how free-surface effects impact maneuvering performance. Carrica et al.[21] conducted numerical simulations of submarine self-propulsion in calm water and in regular waves corresponding to sea states 2-7. However, their study did not specifically focus on the effects of the free surface under both wavy and calm conditions. Chen et al.[22] investigated turning maneuver of a submarine in waves, showing that wave action induces pronounced oscillations in hull attitude.

The coupled effects of the air-water interface, nonlinear wave generation, and unsteady flow fields under free-surface and wave conditions are highly complex, making high-fidelity numerical simulations both challenging and costly. Moreover, under self-propulsion conditions, strong interactions occur among the propeller, control surfaces, hull, free surface, and waves, while the relevant mechanisms and modelling approaches have not yet formed a mature framework. Consequently, research on the influence of waves and free-surface effects on submarine self-propulsion remains relatively limited.

Previous studies have predominantly focused on the self-propulsion response of submarines under fully submerged or calm-water conditions, whereas the coupled effects of the near-surface environment and wave action on self-propulsion attitude, maneuvering characteristics, and hydrodynamic performance have not yet been investigated in a sufficiently comprehensive and systematic manner. To address this gap, the present study considers the Joubert BB2 submarine as the research object and employs an autopilot system to maintain attitude control. The motion response characteristics under different submergence depths and wave conditions are then systematically examined, with the aim of clarifying the mechanisms by which free-surface proximity and waves influence submarine self-propulsion.

1. Numerical methods

1.1 *Governing equations*

In this study, numerical simulations were conducted using the commercial CFD software STAR-CCM+, based on the incompressible RANS equations. The governing equations of RANS are expressed by the continuity equation and the momentum equation, which together describe the fluid flow dynamics. The governing equations are:

$$\frac{\partial \overline{u}_i}{\partial x_i} = 0 \tag{1}$$

$$\frac{\partial \overline{u}_i}{\partial t} + \overline{u}_j \frac{\partial \overline{u}_i}{\partial x_j} = f_i - \frac{1}{\rho}\frac{\partial \overline{p}}{\partial x_i} + \frac{1}{\rho}\frac{\partial}{\partial x_j}\left(\mu \frac{\partial \overline{u}_j}{\partial x_j} - \rho \overline{u_i' u_j'} \right) \tag{2}$$

where t is the time, $\overline{u}_i$ represents the time-averaged velocity components in the Cartesian coordinate system, x_i and x_j are spatial coordinates, the subscripts i and j represent the directions of the coordinate system, taking values of 1, 2, and 3, $\overline{p}$ denotes the time-averaged pressure, μ is the viscosity coefficient, and $\rho \overline{u_i' u_j'}$ represents the Reynolds stresses. The term f_i corresponds to the source term, where the addition of momentum source terms allows for simulating the flow field.

1.2 *Turbulence model*

To close the time-averaged Navier-Stokes equations, various turbulence models are employed to estimate the Reynolds stresses. In this study, the shear stress transport (SST) k-ω turbulence model proposed by Menter is used for closure[7]. This model applies the k-ω formulation to handle boundary layer flows and the k-ε model to address free-stream fluid flows[23]. The transport equations for this model are as follows:

$$\frac{\partial}{\partial t}(\rho k) + \frac{\partial}{\partial x_i}(\rho k u_i) = \frac{\partial}{\partial x_j}\left(\Gamma_k \frac{\partial k}{\partial x_j} \right) + G_k - Y_k + S_k \tag{3}$$

$$\frac{\partial}{\partial t}(\rho \omega) + \frac{\partial}{\partial x_i}(\rho \omega u_i) = \frac{\partial}{\partial x_j}\left(\Gamma_\omega \frac{\partial \omega}{\partial x_j} \right) + G_\omega - Y_\omega + S_\omega \tag{4}$$

where G_k is the production of turbulent kinetic energy, G_ω is the production of specific dissipation rate, Y_k and Y_ω are the respective dissipation terms, S_k and S_ω are the source terms, and Γ_k and Γ_ω are the effective diffusivities.

1.3 *Volume of fluid method*

This study focuses on the self-propulsion motion of submarines near the free surface, which is a typical two-phase flow problem. Therefore, the VOF method is employed to accurately capture the free surface dynamics. This technique was first introduced and developed by Hirt and Nichols[24] in 1981. The principle of the VOF method involves introducing a phase volume fraction α_q (the subscript q denotes the q-th fluid phase), for each fluid to represent the volume fraction of the fluid in any given mesh cell, as expressed by the following equation:

$$\alpha_q = \frac{V_q}{V} \tag{5}$$

where V_q represents the volume of the phase fluid in a given mesh cell. The sum of the volume fractions of all fluid phases within a single mesh cell equals 1, as expressed by the following equation:

$$\sum_{q=1}^{N} \alpha_q = 1 \tag{6}$$

In the two-phase flow problem addressed in this study, only air and water are considered as the two fluid phases. Therefore, the system can be simplified to a single phase volume fraction α. Within a mesh cell, this can be expressed as:

$$\alpha = 0 \text{ Air domain} \tag{7a}$$

$$0 < \alpha < 1 \text{ Interface} \tag{7b}$$

$$\alpha = 1 \text{ Water domain} \tag{7c}$$

The transport equation for the VOF method in the simulation process can be expressed in the following form:

$$\frac{\partial \alpha}{\partial t} + \nabla \cdot (\boldsymbol{U}\alpha) = 0 \tag{8}$$

where $\boldsymbol{U}$ is the fluid velocity vector.

1.4 *Autopilot controller*

The autopilot system employed in this study adjusts the rudder angle based on heading deviation and yaw rate, using a proportional-derivative control system. The control law governing this system is expressed as follows[3]:

$$\delta_{\text{Autopilot}} = P \cdot e(t) + D\frac{\mathrm{d}e(t)}{\mathrm{d}t} \tag{9}$$

where P and D represent the proportional and derivative coefficients, respectively, while $e(t)$ denotes the control term, which is the deviation between the desired and actual values at the current time.

In the self-propulsion simulations conducted in this study, an autopilot controller is implemented to improve control of the attitude of the submarine. The autopilot regulates both horizontal and vertical headings, using heading (yaw) angle as well as depth and pitch angle as the control parameters. Based on the predefined control algorithm, the horizontal and vertical commands are distributed separately to the X-rudders in order to adjust the motion of the submarine accordingly:

$$\delta_{\text{V}}(t) = P_z e(t) + D_z \frac{\mathrm{d}e(t)}{\mathrm{d}t} + P_\theta e(t) + D_\theta \frac{\mathrm{d}e(t)}{\mathrm{d}t} \tag{10}$$

$$\delta_{\text{H}}(t) = P_y e(t) + D_y \frac{\mathrm{d}e(t)}{\mathrm{d}t} + P_\varphi e(t) + D_\varphi \frac{\mathrm{d}e(t)}{\mathrm{d}t} \tag{11}$$

where $\delta_{\text{V}}(t)$ and $\delta_{\text{H}}(t)$ represent the vertical and horizontal rudder commands, respectively, and z, θ, y, and φ denote the heave, pitch, sway, and yaw responses, respectively. For the X-rudders, the rudder command is the combination of the vertical and horizontal rudder commands. The rudder command for each surface is given by the following equation:

$$\delta_{\text{PtUp}} = \delta_{\text{V}} + \delta_{\text{H}}, \delta_{\text{PtDn}} = \delta_{\text{V}} - \delta_{\text{H}} \tag{12}$$

$$\delta_{\text{SbUp}} = -\delta_{\text{V}} + \delta_{\text{H}}, \delta_{\text{SbDn}} = -\delta_{\text{V}} - \delta_{\text{H}} \tag{13}$$

where δ_{PtUp}, δ_{PtDn}, δ_{SbUp}, δ_{SbDn} correspond to the port upper rudder, port lower rudder, starboard upper rudder, and starboard lower rudder, respectively. The rotation of each rudder surface follows the right-hand rule around its rotational axis[10]. Additionally, based on experimental data from Overpelt[3], the maximum rudder angle should not exceed 30°, and the maximum rudder speed is 7.11 (°)/s, which corresponds to a maximum speed of 30.5 (°)/s at the model scale.

2. Numerical setup

2.1 *Geometric models*

The model used in this study is the Joubert BB2 submarine equipped with the Marine 7371R propeller model. All simulations were conducted at the model scale (1:18.348). Table 1 presents the key parameters, and Figure 1 provides an overview of the geometric configuration. The Joubert BB2 submarine is an axisymmetric body of revolution, equipped with a sail, sail rudder, and X-rudders, among other key components. Additionally, it is fitted with the Marine 7371R six-blade propeller. Both the submarine and propeller models were designed by the Netherlands Maritime Research Institute (MARIN)[25-26], which includes the sail, sail rudder, and X-rudders as part of the submarine. The BB2 submarine model is one of the most widely used generic submarine models globally, and it has been extensively applied in hydrodynamic research, including model testing and numerical simulations.

Table 1 The basic parameters of the Joubert BB2 model

Parameters	Value
Length, L / m	3.826
Beam, B / m	0.523
Drought to deck, D / m	0.578
Drought to propeller, D_{P} / m	0.273
Drought to sail, D_{sail} / m	0.883
Displacement ∇ / t	0.703
Longitudinal center of gravity (from nose), x_{CG} / m	1.76
Vertical center of gravity (from shaft), z_{CG} / m	0.286
X- axis moment of inertia, I_{xx} / (kg · m^2)	30.849
Y- axis moment of inertia, I_{yy} / (kg · m^2)	665.448
Z- axis moment of inertia, I_{zz} / (kg · m^2)	665.229

Figure 2 illustrates the two Cartesian coordinate systems used in this study: the spatial coordinate system and the fixed-body coordinate system. In the spatial coordinate system, the coordinates X, Y, and Z are initially aligned with the corresponding axes of the body-fixed coordinate system. The translation and rotational motion within the body-fixed coordinate system are defined by the inertial reference frame of the spatial coordinate system. The origin of the fixed-body coordinate system is located at the center of gravity of the submarine model. In this system, the positive x-axis points toward the bow of the submarine, the positive y-axis points toward the starboard, and the positive z-axis points downward.

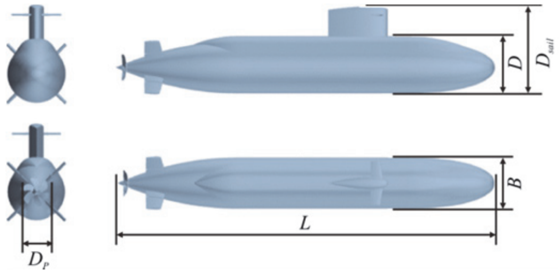

Fig. 1 The Joubert BB2 submarine and Marine 7371R propeller model

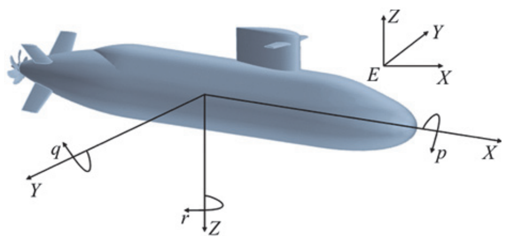

Fig. 2 Space and Body fixed coordinate

2.2 *Computational domain and mesh*

This study focuses on the self-propulsion maneuver performance of the Joubert BB2 submarine near the free surface, and thus the computational domain is divided into the air domain, fluid domain, and free-surface. Figure 3 provides a schematic representation of the computational domain defined for the study.

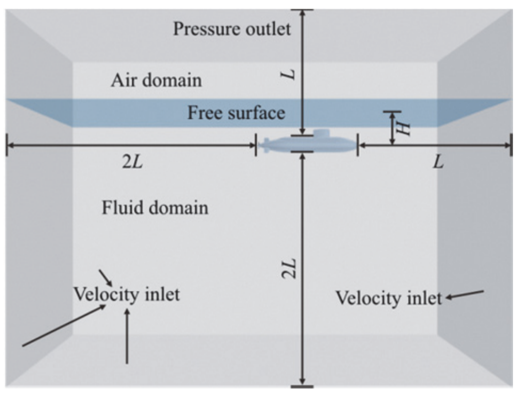

Fig. 3 The computational domain and boundary conditions

The computational domain is modelled as a rectangular block with the submarine located at its center. The domain extends $1L$ (L is the length of the submarine) forward of the bow, $2L$ aft of the stern, and $2L$ in the transverse direction on each side. The distance between the free surface and the geometric center of the hull is defined as the submergence depth H. To reduce the computational cost of the self-propulsion simulations, we adopt a background-domain tracking approach, in which the background domain is translated synchronously with the motion of the submarine. This approach effectively reduces the mesh size and enhances computational efficiency. In the background domain, the upper surface is defined as the pressure outlet, while the remaining five surfaces are designated as velocity inlets. Since wave generation occurs at the free surface during near-surface self-propulsion, a wave absorption method is applied around the background domain to mitigate wave reflection effects.

All meshing in this study was done in the commercial software STAR-CCM+. The meshes are divided into two regions, the hull domain containing the hull and free surface and the rotation domain containing the propeller. The detailed mesh configuration is shown in Fig. 4. In this study, the overset mesh technique is employed to divide the entire computational domain into the background domain, the submarine domain, the X-rudders domain, and the propeller domain. Trimmed Mesh is used in both the hull domain and the rotation domain to perform the mesh dissection operation, and Prism Layer Mesh is used to construct the boundary layer outside the walls of the hull and the propeller, and the number of prism layers on the surface of the hull and the propeller are set to 5 and 3, respectively. Furthermore, the X-rudders domain is meshed using Polyhedral Mesh to ensure its computational accuracy.

Under still water conditions near the free surface, the total number of computational cells is approximately 1.686×10^7. In wave conditions, to more accurately capture the wave characteristics at the free surface, the mesh is further refined, resulting in a total of approximately 2.064×10^7 computational cells.

2.3 *Solvers*

The numerical simulations are performed using a CFD solver based on a cell-centered finite volume discretization in combination with arbitrary polyhedral mesh elements. In the present study, a first-order implicit scheme is adopted for temporal discretization, whereas a second-order upwind scheme is employed for spatial discretization.

To ensure the accuracy of the numerical calculations, it is essential to maintain the Courant number (Co) below 1. Thus, the time step size in the numeri-

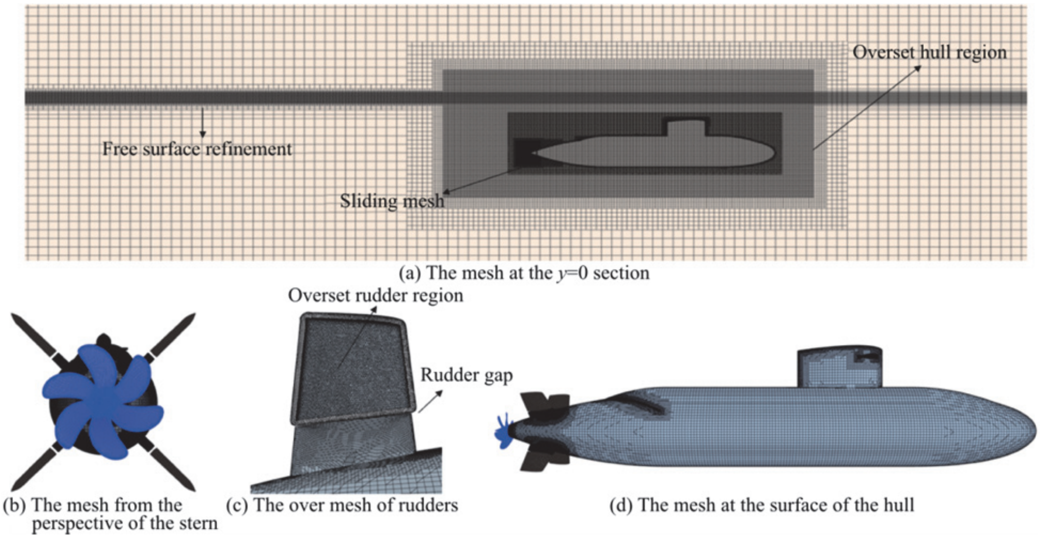

Fig. 4 The overset mesh details for Joubert BB2 submarine

Table 2 The parameters of the mesh configuration

Item	Volume mesh cells×10^6			
	M_1	M_2	M_3	M_4
Background	2.12	5.81	8.09	10.86
Submarine	1.52	4.07	7.04	9.28
Rudder (sbup, sbdown, portup, portdown)	0.04	0.12	0.18	0.24
Propeller	0.12	0.27	1.01	2.08
Total	3.92	10.63	16.86	23.18

cal simulations is typically determined by the Courant number, as indicated by Eq. (14). A time step size of 0.005 was selected to ensure that this criterion is met in most cases:

$$Co = \frac{\delta t \,|U|}{\delta x} \tag{14}$$

where δt is the time step, δx is the length of the mesh in the velocity direction, $|U|$ is the module of the velocity within a certain mesh cell.

3. Numerical validation

3.1 *Mesh convergence study*

Prior to conducting the study, a mesh convergence analysis was performed to determine the appropriate mesh cell size, with the objective of achieving an accurate numerical solution at a lower computational cost. The mesh was progressively refined in all three directions, resulting in four distinct mesh sets. Apart from variations in the mesh cell size, all other parameters remained constant. The meshes were named M_1, M_2, M_3,and M_4 based on the total number of mesh cells, with the corresponding cell counts provided in Table 2.

Figure 5 shows the results of mesh convergence study. The mesh convergence study was conducted under still water conditions for near-surface self-propulsion. Numerical simulations were performed for four different mesh sets at a submergence depth of $H/L = 0.27$, with the flow field reaching stability before comparing the thrust at the self-propulsion point. Based on the computational results from four mesh sets and considering both computational cost and convergence, all numerical simulations in this study were conducted using the M_3 mesh.

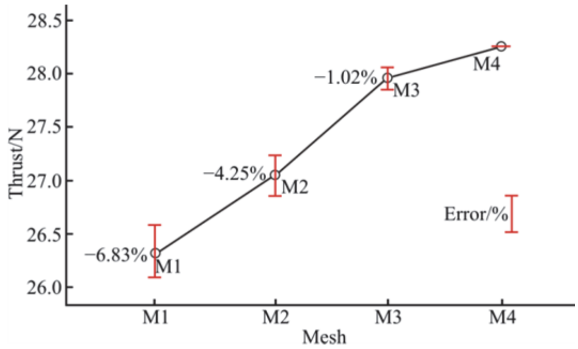

Fig. 5 The results of mesh convergence study

3.2 *Self-propulsion validation*

In the absence of experimental data for self-propulsion near the free surface, a preliminary verification was first carried out for the self-propulsion performance in the fully submerged condition to assess the validity of the numerical model. The present simulation adopted the same parameters as those used in the self-propulsion model tests of Overpelt et al.[3]: The target cruising speed of the model was set to 1.2 m/s, and an autopilot with identical control settings was employed to regulate attitude during self-propulsion. The numerical results in the fully submerged case were then evaluated and compared with the CFD results reported by Han et al.[16].

Table 3 summarizes the results of self-propulsion validation. Compared with the experimental data, the thrust error at the self-propulsion point is only 3.38%, and the propeller rotational speed error is about 2.98%. In addition, the predicted propeller rotating speed is almost identical to that reported by Han et al., with a discrepancy of approximately 1.47%, indicating that the present CFD approach can accurately reproduce realistic self-propulsion behavior. The discrepancy in thrust relative to the results of Han et al. is approximately 4.96%, which may be attributed to the fact that a body-force propeller model was adopted in their simulations, whereas the present study employs the sliding-mesh approach to represent the actual propeller rotation more realistically.

Table 3 Results of self-propulsion validation

Parameters	Thrust/N	Rotating speed/rpm
Experiment[3]	26.6	268
CFD[16]	26.2	272
Present	27.5	276
Error (exp. vs present)	3.38%	2.98%
Error (Han's vs present)	4.96%	1.47%

Table 4 Simulation conditions

Case	H/L	Environment
1	Submerged	Calm water
2	0.18	Calm water
3	0.23	Calm water
4	0.27	Calm water
5	0.18	Regular wave
6	0.23	Regular wave
7	0.27	Regular wave

4. Results and discussions

This section presents the self-propulsion results for the Joubert BB2 submarine model under different submergence depths in both calm water and wave environments. All key results are presented in a dimensionless form based on the model scale, corresponding to a speed of $U_0 = 1.2$ m/s (10 kn in full scale). Furthermore, Table 4 shows the simulation conditions, wherein the submergence depth (H/L) under different operating conditions is defined as the ratio of the distance (H) between the axis of submarine and the free surface to the length (L) of the submarine. This ratio corresponds to the nominal submergence depth of the submarine. The regular wave considered in this study have a wave period T of approximately 1.6 s, a wavelength λ of 4.0 m, and an amplitude a_0 of 0.1 m.

4.1 *Near-surface self-propulsion*

Figure 6 presents the time histories of the velocity and pitch angle at different submergence depths, along with the real-time rudder deflection signals of the X-rudders controlled by the autopilot during self-propulsion, where δ_{su} and δ_{sd} denote the Starboard-Up Rudder Angle and Starboard-Down Rudder Angle, respectively. During the initial stage of motion, the flow field around the hull has not yet fully developed, and the non-uniform pressure distribution between the bow and stern generates a pronounced pitching moment, which in turn induces a relatively large pitch angle. The autopilot then intervenes and rapidly applies control actions, with the resulting control moment suppressing any further increase in attitude deviation. Once the motion enters the steady self-propulsion stage, however, the inherent characteristics of the PD control algorithm make it difficult to eliminate the steady-state error completely. As a result, the hull eventually reaches equilibrium at a small but finite constant pitch angle. The results indicate that under the control of the autopilot, the submarine maintains a stable sailing posture and achieves the desired self-propulsion speed. When the submergence depth is $H/L = 0.18$, the additional hydrodynamic resistance caused by the hull's proximity to the free surface results in a slightly lower steady self-propulsion speed compared with the nominal speed. Furthermore, the time history of the pitch angle reveals the final pitching trend during near-surface self-propulsion. At $H/L = 0.18$, the maximum pitch angle reaches approximately 1.37°. At submergence depths of $H/L = 0.23$ and $H/L = 0.27$, the steady-state pitch angles are nearly identical to those observed in the fully submerged condition. This indicates that when the submergence depth exceeds $H/L = 0.23$, the free-surface effect has only a negligible influence on the submarine attitude during self-propulsion. Specifically, at submergence depths of $H/L = 0.23$, $H/L = 0.27$ and under the fully submerged condition the steady pitch angles are 0.07°, 0.05°, and 0.03°, all of which are close to 0°, while at $H/L = 0.18$, the steady pitch angle reaches approximately 0.38°. The stabilizing moment required to achieve steady direct navigation is achieved by the autopilot controlling the X-rudders, with the rudder angle changes during the control process corresponding to the pitch angle.

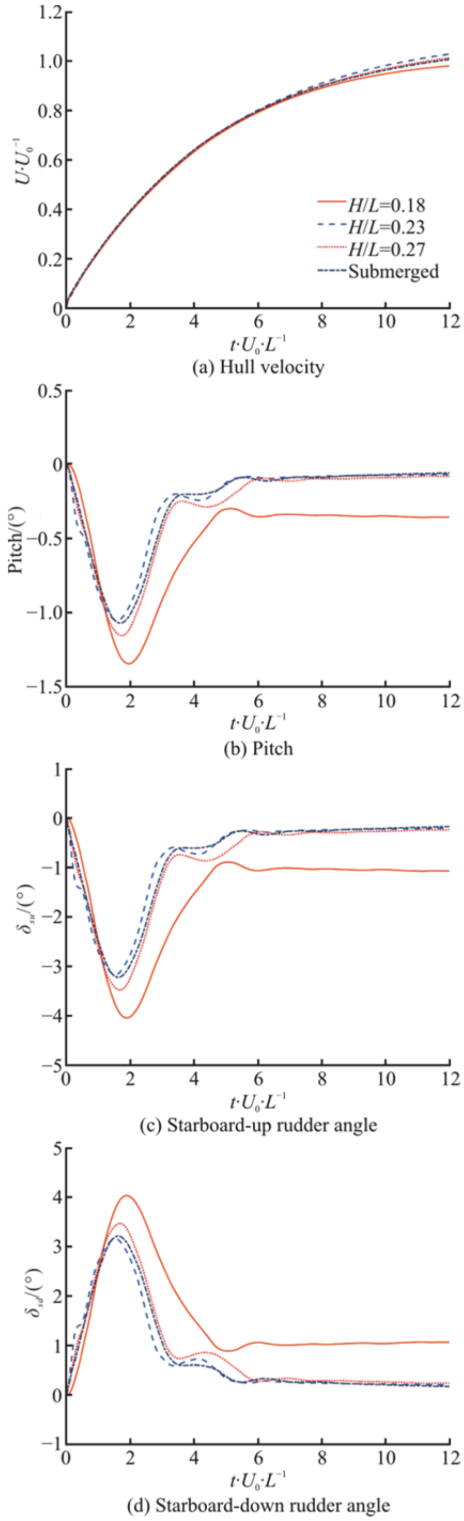

Fig. 6 Hull velocity, Pitch and Rudder deflection for self-propulsion near the surface

It is noteworthy that the deflection values of the X-rudders surfaces for the port-up and starboard-down as well as port-down and starboard-up configurations are always equal in magnitude but opposite in direction, as indicated by the control commands mentioned in the previous section. Therefore, the following presents the tailplane angles for the starboard-up and starboard-down configurations calculated by the autopilot during the stable self-propulsion phase to maintain the submarine attitude. When the submergence depth of the submarine is $H/L = 0.18$, the maximum rudder deflection of the X-rudders reaches approximately 4°, in order to maintain the heading posture with the hull proximity to the water surface.

As shown in Fig. 7, 8, where streamlines and solid surfaces are colored using the pressure coefficient C_p, which is defined as follows:

$$C_p = \frac{P - \rho g h}{0.5 \rho U^2} \tag{15}$$

where $P - \rho g h$ denotes the definition of dynamic pressure, ρ represents fluid density, and U indicates the submarine speed.

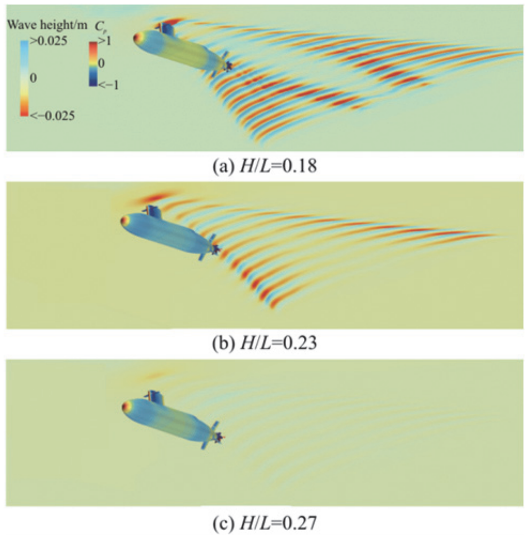

Fig. 7 Self-propulsion of Joubert BB2 near the surface

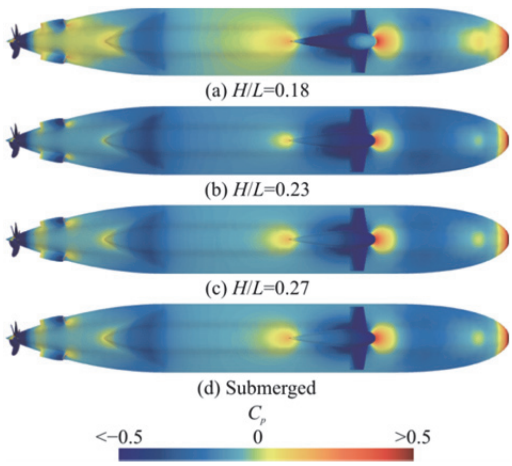

Fig. 8 Dynamic pressure distribution on the top surface of submarines at the self-propulsion motion

It is evident that during self-propulsion, significant high-pressure regions are observed at the forward and central portions of the hull, while the stern exhibits a low-pressure area due to the suction effect generated by the propeller rotation. This results in a slight bow pitch angle as the submarine maintains stable self-propulsion. Additionally, the pressure distribution on the hull varies with submergence depth. At $H/L=0.18$, the hull's proximity to the free surface leads to the formation of high-pressure zones along the proximity sections. In contrast, at $H/L=0.27$, the pressure distribution becomes nearly identical to that of a fully submerged condition, indicating that the influence of the free surface on the submarine is minimal when the submergence depth exceeds this value.

Figure 9 presents the time histories of thrust and torque during the near-surface self-propulsion of the submarine. As the submarine speed gradually converges to U_0, both thrust and torque also stabilize. It is observed that as the submergence depth increases, the steady-state thrust and torque values decrease.

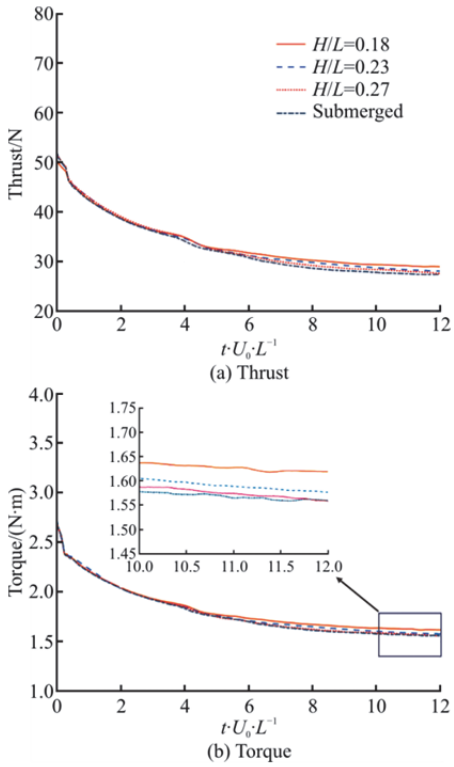

(a) Thrust

(b) Torque

Fig. 9 Thrust and torque for self-propulsion near the surface

Specifically, at a near-surface depth of $H/L=0.18$, compared with the fully submerged condition, the thrust increases by approximately 8.9%, and the torque increases by approximately 3.8%. At $H/L=0.23$, the thrust is about 3.5% higher, and the torque increases by roughly 1.2% relative to the fully submerged condition. At $H/L=0.27$, the thrust and torque are nearly identical to those of the fully submerged state, indicating that, beyond this submergence depth, the effect of the free surface on the submarine's propulsion performance becomes negligible.

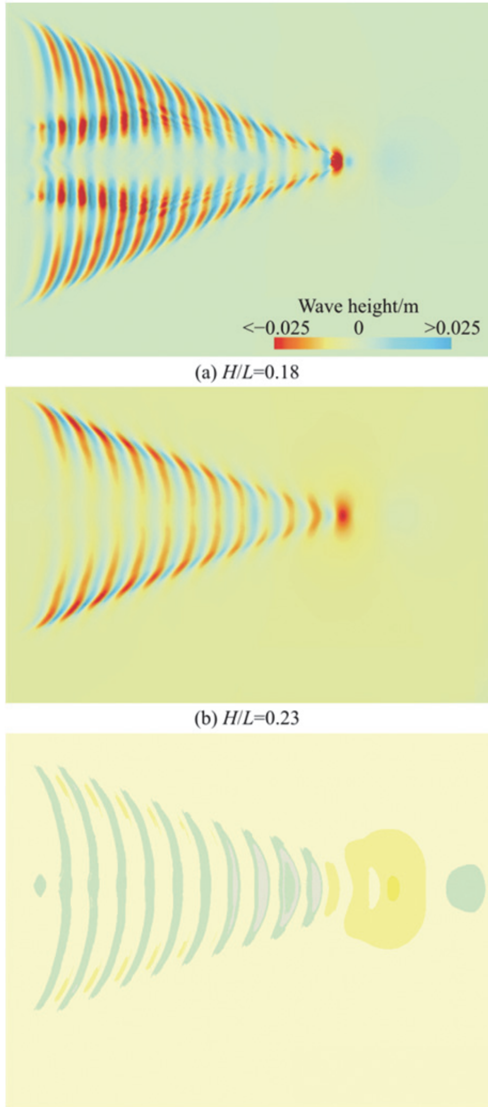

(a) $H/L=0.18$

(b) $H/L=0.23$

(c) $H/L=0.27$

Fig. 10 Waveform during self-propulsion motion near the surface

When the submarine performs self-propulsion near the free surface, surface waves are generated. Previous studies have shown that submarines operating near the free surface produce Kelvin wave systems[20]. Figure 10 illustrates the free-surface wave patterns generated during the submarine self-propulsion. A distinct wave trough is observed near the aft section of the sail, where wave formation is particularly strong and the wave height is considerable. This phenomenon arises primarily from the pressure gradient change as the fluid flows past the sail, resulting in a wake field that interacts with the free surface. A second region of significant wave formation occurs behind the propeller, where a pronounced wave crest with considerable height is formed. This is another region where wave generation is intense, mainly due to the high-speed wake generated by the rotating propeller interacting with the free surface.

Under the same speed conditions, when the submergence depth is shallow i.e. closer to the free surface, the generated wave height is larger. Additionally, the coupling effects between scattered waves and transverse waves become more pronounced. In contrast, at deeper submergence depths, the wave height decreases, the scattered wave effects become less noticeable, and only the characteristics of transverse waves remain. This suggests that the submarine's influence on the free surface diminishes as the submergence depth increases. It is noteworthy that at submergence depths of $H/L=0.18$ and $H/L=0.23$, the sail is in very close proximity to the free surface. This results in the accumulation of incoming waves at the front of the sail, which then separate towards the wings. A region of significantly reduced wave height appears along the submarine's central axis.

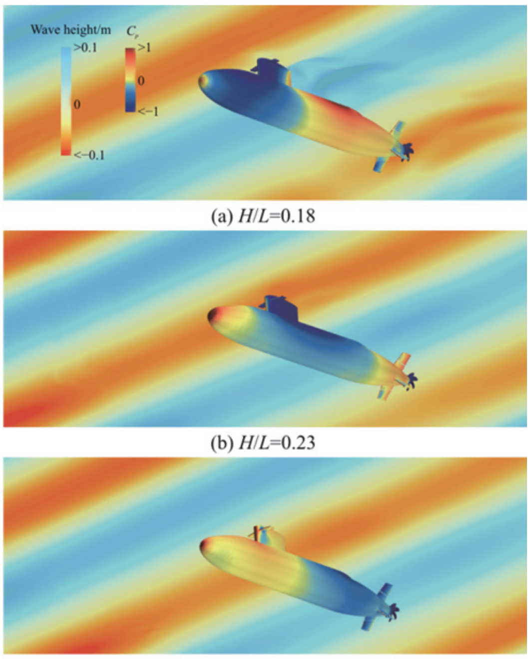

(a) H/L=0.18

(b) H/L=0.23

(c) H/L=0.27

Fig. 11 Self-propulsion of Joubert BB2 near the surface in wave

4.2 *Self-propulsion in waves*

This section analyzes the effects of different submergence depths on the kinematic and dynamic parameters of the Joubert BB2 during self-propulsion in wave conditions. Figure 11 illustrates the self-propulsion state of the Joubert BB2 at various submergence depths in near-surface wave environments. Figure 12 presents the time histories of velocity and pitch angle, as well as the real-time rudder deflection signal of the X-rudders controlled by the autopilot during self-propulsion at different submergence depths under wave conditions.

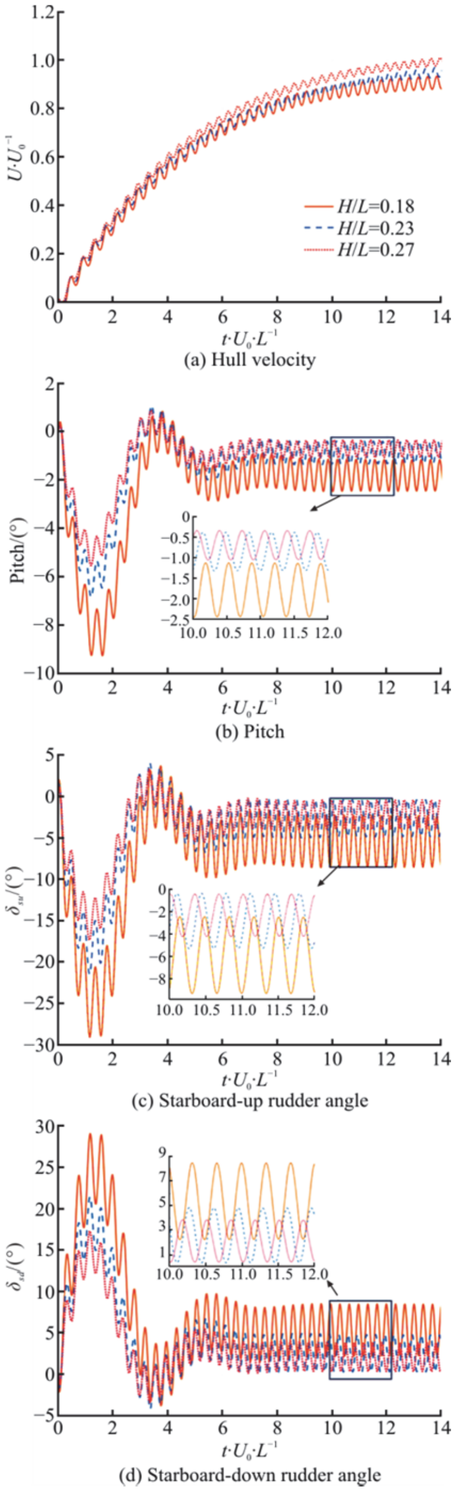

Fig. 12 Hull velocity, Pitch and Rudder deflection for self-propulsion near the surface in wave

The presence of waves imposes unsteady, periodic wave loads on the submarine hull, resulting in pronounced periodic fluctuations in both attitude and speed. The amplitudes of these fluctuations decrease progressively with increasing submergence depth. Compared with self-propulsion in calm water, the additional hydrodynamic resistance caused by the waves results in a slightly lower steady-state velocity at shallower submergence depths, with the velocity stabilizing slightly below the nominal speed U_0. At a submergence depth of $H/L=0.27$, the influence of waves on the submarine is minimal, allowing the velocity to converge well to U_0.

Under wave conditions, the pitch angle of the submarine undergoes significant fluctuations during self-propulsion. At a submergence depth of $H/L=0.18$, the steady-state time-averaged pitch angle reaches 1.88°, which is around five times that under calm-water conditions. As the submergence depth increases, the pitch attitude gradually becomes more stable; however, periodic oscillatory behavior remains evident under wave-induced disturbances. At $H/L=0.23$ and $H/L=0.27$, the steady-state pitch angles are 0.92° and 0.73°, respectively. Although these values are reduced relative to the shallower free-surface condition, they remain markedly higher than the corresponding calm-water values of 0.07° and 0.05°. These results indicate that the wave environment substantially amplifies attitude deviation and makes it more difficult to maintain a stable running attitude.

Under the control of the autopilot, the X-rudders adjust the submarine's attitude by calculating the required rudder deflection and executing the necessary steering commands. The variations in the rudder deflection are directly correlated with changes in the submarine's attitude. During the initial phase, the submarine experiences significant attitude changes, which leads to larger initial rudder deflection commands from the autopilot. For instance, at a submergence depth of $H/L=0.18$, the maximum rudder angle of the X-rudders may exceed 25° in order to compensate for the initial significant pitch angle and maintain the Joubert BB2's steady attitude-keeping posture.

Figure 13 presents the time histories of thrust and torque during the self-propulsion of the Joubert BB2 submarine in near-surface wave environments. Similar to the trends observed in calm water, both thrust and torque decrease as the submergence depth increases. However, the presence of waves induces significant periodic fluctuations in both thrust and torque. These fluctuations become less pronounced as the submergence depth increases. At the near-surface submergence depth of $H/L=0.18$, the thrust increases by approximately 5.71%, and the torque increases by around 1.26%, compared with the $H/L=0.27$ condition. The thrust and torque at $H/L=0.23$ are slightly higher than those at $H/L=0.27$, but the fluctuations in both thrust and torque are more pronounced.

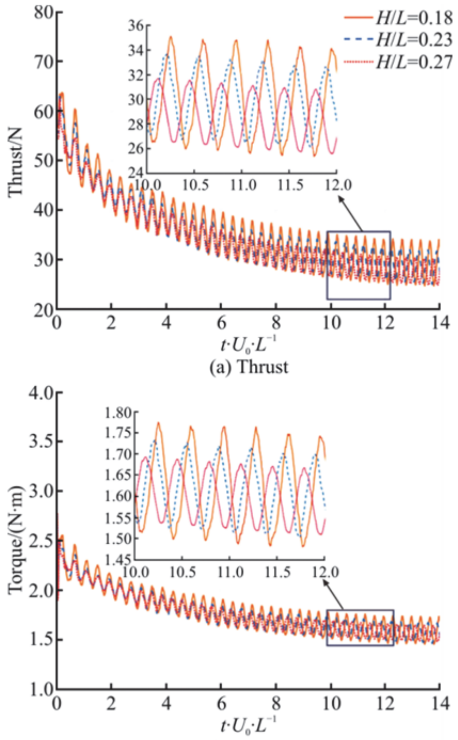

Fig. 13 Thrust and torque for self-propulsion near the surface in wave

As shown in Fig. 14, where streamlines and solid surfaces are colored using the dimensionless resultant velocity U', which is defined as follows:

$$U' = \frac{U_{\text{Hull}}}{U_0} \tag{16}$$

It is observed that the main velocity wake is formed downstream of the propeller. The interaction between the free-surface waves and the sail modifies the flow in the region between the sail and the free surface, leading to a distinct high-velocity region immediately downstream of the sail. In contrast, the flow field beneath the submarine remains relatively unchanged. Notably, at $H/L=0.18$, the interaction with the free surface is most pronounced, leading to a significant high-velocity region both fore and aft of the sail. This interaction causes increased wave disturbances and more intense velocity fluctuations.

As the submergence depth increases to $H/L=0.23$ and $H/L=0.27$, the influence of the free surface diminishes, and the velocity distribution stabilizes. The low-velocity regions shrink, and the propeller wake, along with the overall flow field around the submarine, becomes more stable. Additionally, it is evident from the images that as the submergence depth approaches the free surface, the pitch amplitude of the Joubert BB2 submarine increases. This suggests that the closer the submarine is to the free surface, the greater the pitch variations during self-propulsion.

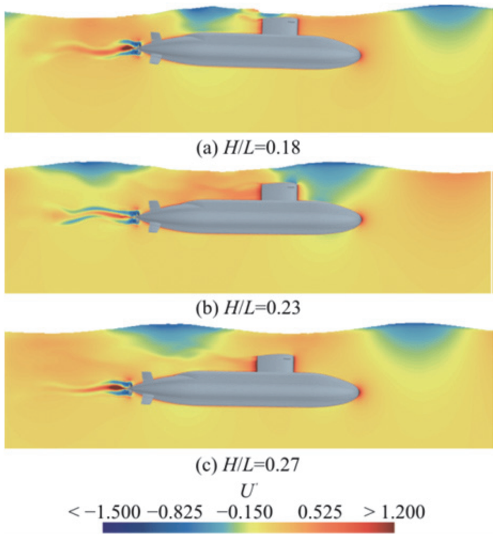

Fig. 14 The instantaneous views for the dimensionless resultant velocity at the center plane

5. Conclusions

In this study, the commercial software STAR-CCM+ was used to develop a numerical simulation method for near-surface self-propulsion of a submarine based on an overset mesh approach. The self-propulsion motion of the Joubert BB2 submarine at various submergence depths was simulated in both free-surface and wave environments to assess the impact of the free surface and waves on the hydrodynamic characteristics of the submarine self-propulsion. The conclusions derived from the analysis of the computational results are summarized as follows:

(1) A CFD simulation method for analyzing the self-propulsion motion of submarines has been developed. This method employs an overset mesh approach to model the submarine and its four rudders, while the sliding mesh technique is used to simulate the rotation of the propeller. The autopilot system is utilized to control the horizontal and vertical motion attitude errors of the submarine during self-propulsion. The simulation results were compared with experimental data under the same conditions, showing a thrust error of 3.38% and a propeller speed error of 2.98%. These results indicate a good agreement between the CFD simulations and the experimental data, validating the accuracy of the simulation method.

(2) As the submergence depth increases, the wave-making resistance of the submarine decreases, and the thrust and torque required for steady self-propulsion are reduced accordingly. When the submarine operates near the free surface, its pitch angle under autopilot control is noticeably greater compared with submerged conditions. The autopilot system compensates for the free-surface effects by applying larger rudder angles to maintain the desired attitude. Additionally, the value of hull velocity is slightly reduced in near-surface conditions compared with submerged condition, indicating a slight decrease in stability during self-propulsion at shallow depths.

(3) When the submarine operates under near-surface wave conditions in self-propulsion, the waves impose unsteady, periodic loads on the hull, leading to pronounced oscillations in attitude and forward speed. Moreover, the influence of the waves results in a significant increase in the vertical attitude compared with that in calm water conditions. To mitigate errors in vertical motion attitude, the autopilot system generates rudder commands that exhibit distinct periodic fluctuations. As the submergence depth increases, the amplitude of fluctuations in speed, pitch, and rudder angles decreases, indicating a reduction in the impact of unsteady wave forces on the submarine motion.

It should be noted that the present study is primarily concerned with the self-propulsion behavior of a submarine in free-surface and regular-wave environments, and does not yet address the response characteristics associated with other representative maneuvers, such as turning and Zigzag maneuvering, under free-surface and wave conditions. In addition, only a single regular-wave condition is considered in the present work. Future research will therefore extend the numerical investigation to more complex maneuvering motions in waves, including turning and Zigzag maneuvering, and will systematically examine the effects of different wavelengths, wave heights, submergence depths, and irregular-wave conditions on submarine maneuvering performance and attitude response.

Conflict of interest

All authors declare that there are no other competing interests.

References

[1] Hess D, Fu T. Impact of flow control technologies on naval platforms [C]. *Proceedings of the 33rd AIAA Fluid Dynamics Conference and Exhibit*, Orlando, Florida, USA, 2003.

[2] Hess D, Fu T, Cubbage S. Naval maneuvering research and the need for shear stress measurements [C]. *Proceedings of the 48th AIAA Aerospace Sciences Meeting Including the New Horizons Forum and Aerospace Exposition*, Orlando, Florida, USA, 2010.

[3] Overpelt B, Nienhuis B, Anderson B. Free running manoeuvring model tests on a modern generic SSK class submarine (BB2) [C]. *Proceedings of the Pacific International Maritime Conference*, Sydney, Australia, 2015.

[4] Özden Y A, Özden M C, Demir E, et al. Experimental and numerical investigation of DARPA Suboff submarine propelled with INSEAN E1619 propeller for self-propulsion [J]. *Journal of Ship Research*, 2019, 63(4): 235-250.

[5] Wang L, Martin J E, Felli M, et al. Experiments and CFD for the propeller wake of a generic submarine operating near the surface [J]. *Ocean Engineering*, 2020, 206: 107304.

[6] Bai T, Wu Y, Wei P, et al. Numerical simulation of submarine self-propulsion based on different turbulent simulation models [C]. *Proceedings of the 38th International Conference on Offshore Mechanics and Arctic Engineering*, Glasgow, Scotland, UK, 2019.

[7] Menter F R. Two-equation eddy-viscosity turbulence models for engineering applications [J]. *AIAA Journal*, 1994, 32(8): 1598-1605.

[8] Liefvendahl M, Troëng C. Computation of cycle-to-cycle variation in blade load for a submarine propeller using LES [C]. *Proceedings of the 2nd International Symposium on Marine Propulsors*, Hamburg, Germany, 2011.

[9] Posa A, Balaras E. Large-eddy simulations of a notional submarine in towed and self-propelled configurations [J]. *Computers & Fluids*, 2018, 165: 116-126.

[10] Carrica P M, Kerkvliet M, Quadvlieg F, et al. CFD simulations and experiments of a submarine in turn, zigzag, and surfacing maneuvers [J]. *Journal of Ship Research*, 2021, 65(4): 293-308.

[11] Lungu A. A DES-based study of the flow around the self-propelled DARPA Suboff working in deep immersion and beneath the free-surface [J]. *Ocean Engineering*, 2022, 244: 110358.

[12] Chase N, Carrica P M. Submarine propeller computations and application to self-propulsion of DARPA Suboff [J]. *Ocean Engineering*, 2013, 60: 68-80.

[13] Sezen S, Dogrul A, Delen C, et al. Investigation of self-propulsion of DARPA Suboff by RANS method [J]. *Ocean Engineering*, 2018, 150: 258-271.

[14] Cheng L, Lu H, Guo B, et al. Fast prediction of underwater vehicle motion under internal solitary waves [J]. *Physics of Fluids*, 2026, 38(2): 022127.

[15] Kim H. Six-DOF motion response and manoeuvring simulation of an underwater vehicle [D]. Doctoral Thesis, Hobart, Australia: University of Tasmania, 2018.

[16] Han K, Cheng X, Liu Z, et al. Six-DOF CFD simulations of underwater vehicle operating underwater turning maneuvers [J]. *Journal of Marine Science and Engineering*, 2021, 9(12): 1451.

[17] Cao L, Gao G, Guo E, et al. Hydrodynamic performances and wakes induced by a generic submarine operating near the free surface in continuously stratified fluid [J]. *Journal of Hydrodynamics*, 2023, 35(3): 396-406.

[18] Guo H, Liu Y, Ge J, et al. Numerical investigation on the turning motion of a near-surface self-propelled submarine [J]. *International Journal of Naval Architecture and Ocean Engineering*, 2025, 18: 100718.

[19] Chen M, Zhang N, Zheng W, et al. Numerical simulation of near-surface turn maneuver of a generic submarine [J]. *Ocean Engineering*, 2023, 287: 115835.

[20] Guo E, Wang Y, Cao L, et al. Numerical investigation on steady turning motion of a generic submarine near the free surface [J]. *Ocean Engineering*, 2024, 313: 119375.

[21] Carrica P M, Kim Y, Martin J E. Near-surface self propulsion of a generic submarine in calm water and waves [J]. *Ocean Engineering*, 2019, 183: 87-105.

[22] Chen M, Zhang N, Chen J, et al. Numerical simulation of near-surface turn maneuver of a submarine in waves [J]. *Physics of Fluids*, 2024, 36(7): 075139.

[23] Zhang M, Hu H, Guo B, et al. Predicting shear stress distribution on structural surfaces under internal solitary wave loading: A deep learning perspective [J]. *Physics of Fluids*, 2024, 36(3): 035154.

[24] Hirt C W, Nichols B D. Volume of fluid (VOF) method for the dynamics of free boundaries [J]. *Journal of Computational Physics*, 1981, 39(1): 201-225.

[25] Petrov V, MacLin G, Cichella V. Underwater vehicle autopilot system for controlling depth and pitch: Maneuvering through near-surface waves and environmental disturbances [J]. *Ocean Engineering*, 2025, 317: 119910.

[26] Li L, Wang Y, Cao L, et al. Reducing internal solitary wave–induced motions of a self-propelled submarine via PD–PI autopilot control [J]. *Ocean Engineering*, 2026, 356: 125401.